Geochemistry, Geophysics, Geosystems

RESEARCH ARTICLE
10.1029/2020GC009383

Sulfur Cycling During Progressive Burial in Sulfate-Rich Marine Carbonates

Lei Jiang[1,2,3,4], Mojtaba Fakhraee[5], Chunfang Cai[1,3], and Richard H. Worden[6]

[1]Key Laboratory of Cenozoic Geology and Environment, Institute of Geology and Geophysics, Chinese Academy of Sciences, Beijing, China, [2]State Key Laboratory of Lithospheric Evolution, Institute of Geology and Geophysics, Chinese Academy of Sciences, Beijing, China, [3]Innovation Academy for Earth Science, Chinese Academy of Sciences, Beijing, China, [4]College of Resources and Environment, China University of Geosciences, Wuhan, China, [5]The Department of Earth & Planetary Sciences, Yale University, New Haven, Connecticut, USA, [6]Department of Earth Ocean and Ecological Sciences, School of Environmental Sciences, University of Liverpool, Liverpool, Merseyside, UK

Abstract The isotopic composition of sulfate in the rock record has been frequently used to track the changes in the Earth's surface environments. By considering isotopic fractionation imparted by microbial sulfate reduction (MSR) and thermochemical sulfate reduction (TSR), in this study, we aim to develop a holistic understanding of the mixed effects of MSR and TSR on $\delta^{34}S$ signals in sulfate-rich carbonate systems. We report the occurrence of various types of sulfur-bearing components from the Cambrian-Ordovician carbonate system in the Tarim Basin, NW China, coupled with a well-established diagenesis framework for these rocks. Our results indicate that most of the sulfur-bearing species possess $\delta^{34}S$ values slightly lower than both the source sulfate and the sulfide generated by TSR, yet these sulfur-bearing species have substantially higher $\delta^{34}S$ values than sulfide that resulted from MSR. Hence, a combination of sulfides sourced from MSR and TSR can adequately explain the sulfur isotope data in the studied interval. Building upon this hypothesis, we developed a new sulfur diagenesis model in order to quantify the accumulated H_2S from the combined effects of MSR and TSR. Our new model can be used to explain the origin of sulfur-bearing species in many other deep burial carbonate systems, including the Sichuan Basin, China, and the Gulf of Mexico, USA. We propose that greater attention should be paid to isotopic modulation through mixed diagenetic processes in order to gain a better mechanistic understanding of the primary geochemistry signals (e.g., $\delta^{34}S$) in marine carbonates.

Key Points:

- A new sulfur cycling diagenesis model was built based on sulfur-bearing species generated during progressive burial
- This new model advanced the quantification of accumulated H_2S from sulfate reductions in many global deep burial basins
- This new sulfur cycling model can be used to better define the origins of superheavy pyrite commonly present in the Neoproterozoic Era

Supporting Information:

- Supporting information S1

Correspondence to:
Lei Jiang,
lei.jiang@mail.iggcas.ac.cn

Citation:
Jiang, L., Fakhraee, M., Cai, C. F., & Worden, R. H. (2020). Sulfur cycling during progressive burial in sulfate-rich marine carbonates. *Geochemistry, Geophysics, Geosystems*, *21*, e2020GC009383. https://doi.org/10.1029/2020GC009383

Received 17 AUG 2020
Accepted 16 OCT 2020

1. Introduction

The sulfur isotopic composition ($\delta^{34}S$) of sedimentary sulfate and sulfide are routinely used to infer the evolution of Earth's surface environment, for example, varying atmospheric oxygen concentrations, the oxidation state of the oceans, and episodes of metazoan evolution and mass extinction (Fike et al., 2015; Lyons et al., 2014). Specifically, due to limited isotopic fractionation (0%–2%) during sulfate mineral crystallization and dissolution (Holser & Kaplan, 1966; Thode & Monster, 1965), the isotopic composition of sedimentary marine evaporites is widely used as a faithful proxy for the reconstruction of paleo-seawater chemistry (Claypool et al., 1980). In addition to sedimentary evaporites, the sulfur isotopic composition of sedimentary sulfide (e.g., pyrite), as an end product of the reduction of sulfate to sulfide in anoxic settings, plays a crucial role in paleoclimate reconstruction (Fike et al., 2015; Lyons et al., 2014).

Sedimentary sulfide can generally be formed through microbial sulfate reduction (MSR) at low temperatures or high temperatures through thermochemical sulfate reduction (TSR). In the modern marine sediments and hydrothermal systems, MSR is viewed as being predominant, with ^{34}S depletions of up to 72% in the reduced sulfur compared to marine sulfate (Böttcher et al., 1999; Bradley et al., 2016; Canfield & Teske, 1996; Jørgensen, 1990; Sim et al., 2011; Wortmann et al., 2001). Sulfur cycling by MSR occurs immediately after marine sedimentation, for example, by organic matter sulfurization (Shawar et al., 2018), during very early diagenesis stage (Jiang et al., 2019), and continues up to a burial temperature of about 100°C (Figure 1; Machel, 2001). By contrast, TSR which commonly occurs at relatively high temperatures (>100°C) in carbonate-hosted petroleum systems, appears to impart little (mostly <2%) sulfur isotope

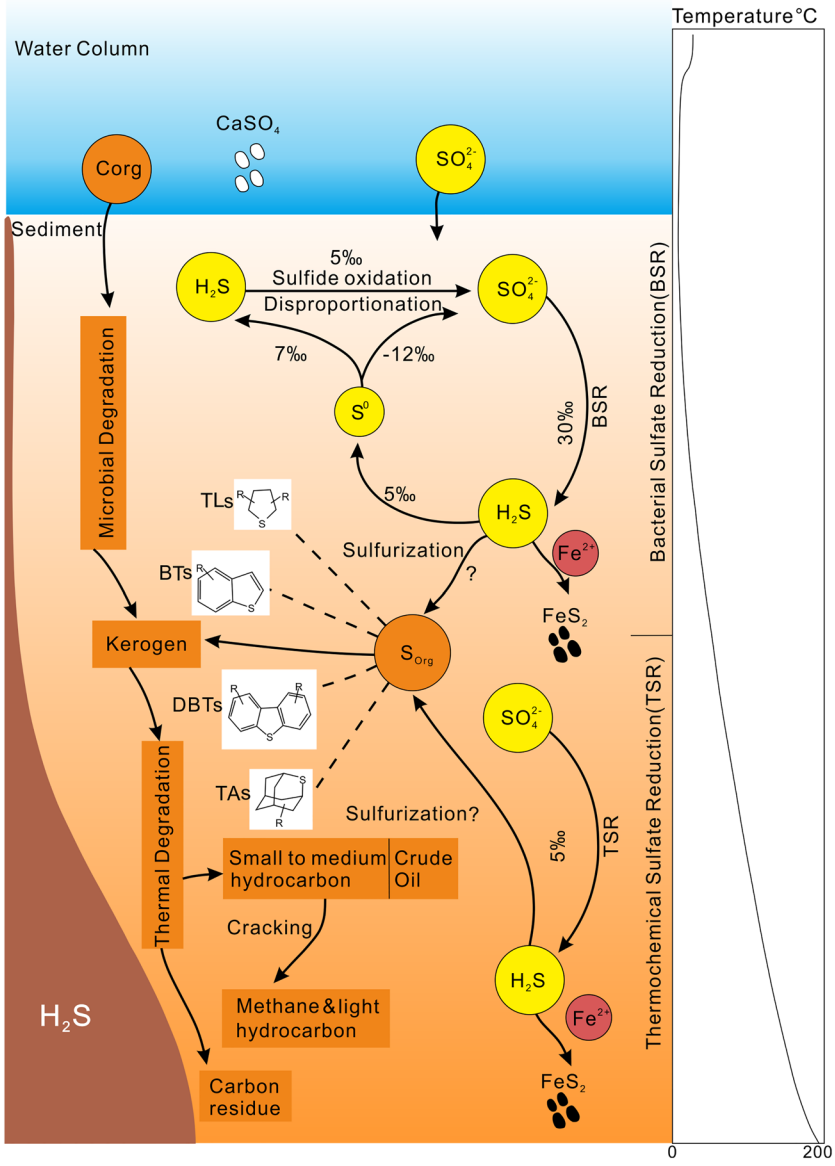

Figure 1. Conceptual depiction of sulfur cycling diagenesis under different burial temperature regimes. Different isotope fractionation (Fike et al., 2015; Worden et al., 1997) resulted from the reduction of sulfate at two different temperature regimes (MSR and TSR) result in sedimentary sulfide with two distinct isotope fractionation. BTs, benzothiophenes; DBTs, dibenzothiophenes; MSR, microbial sulfate reduction; TAs, thiaadamantanes; TLs, thiolanes; TSR, thermochemical sulfate reduction.

fractionation in sulfate-rich carbonate systems (Figure 1; Cai et al., 2015a; Krouse et al., 1988; Worden et al., 1997), although some lab experiments suggest large isotope fractionation during TSR (>10%; Kiyosu, 1980; Kiyosu & Krouse, 1990).

Transformation of sulfur between different species can complicate the interpretation of the $\delta^{34}S$ in the rock records. More precisely, sedimentary sulfate can be completely dissolved or transformed into other sulfur-bearing species, such as H_2S, sulfide minerals, elemental sulfur, and organosulfur species through diagenesis (Bildstein et al., 2001). When sedimentary sulfate is completely transformed to reduced sulfur-bearing phases through TSR, due to limited isotope fractionation, the reduced S may provide useful information about the contemporaneous marine sulfate (Worden et al., 1997). The reduced sulfur that results from MSR, however, may not provide useful information about sedimentary sulfate, owing to the highly var-

iable sulfur isotope fractionation during MSR (Canfield & Thamdrup, 1994; Sim et al., 2011). Experimental studies have demonstrated that the isotopic fractionation (ε) associated with MSR varies with sulfate concentration and organic matter availability (Bradley et al., 2016; Fike et al., 2015; Wing & Halevy, 2014). In modern sediments, it has been shown that the sulfur isotopic offset between seawater sulfate and preserved mineral sulfides is predominantly controlled by whether MSR occurred in a closed or open system (Bryant et al., 2019; Claypool, 2004; Jorgensen, 1979; Masterson et al., 2018). Additionally, mixing of the reduced sulfur-bearing species (e.g., elemental sulfur, H_2S, pyrite) generated from MSR and TSR diagenesis, and the different sulfate reduction rate in specific carbonate systems in diverse sedimentary basins, add more complexity to the interpretation of S-isotope data. Hence, recognition of the origin of the various types of sulfur-bearing species and their sulfur isotopic compositions is paramount in understanding the sulfur cycling during diagenesis. Herein, we consider various regimes of carbonate diagenesis (Worden et al., 2018): (1) surface diagenesis, occurring within centimeters to a few meters of the sediment surface, (2) eodiagenesis, occurring from a few centimeters to depths where temperatures are equal to about 60°C–70°C, and (3) mesodiagenesis, where temperatures exceed 70°C. These temperatures approximately relate to the regimes under which sulfate reduction happens since MSR can occur up to about 70°C–80°C and TSR commences at temperatures greater than 100°C.

In this study, we present new sulfur isotope data from sedimentary sulfate and various types of pyrite in hydrocarbon-hosting, Cambrian-Ordovician (Cam-Ord), carbonate sediments, from the Tarim Basin in China (Figure 2), from which these S-bearing phases have been previously shown to be the products of eodiagenesis and mesodiagenesis (Jia et al., 2015; Jiang et al., 2015a, 2018a; Figure S1). Published $\delta^{34}S$ values of H_2S (gas phase), oil, kerogen, and barite (Cai et al., 2015a, 2016), $\delta^{34}S$ values of diagenetic anhydrite (Jia et al., 2015), and $\delta^{34}S$ values of aqueous sulfate (Li et al., 2017), were also incorporated in order to build a new and holistic sulfur diagenesis model. Applied to other sulfate-rich carbonate systems, this new model offers a revised explanation for the possible origin of various types of sulfur-bearing species in a range of Phanerozoic carbonates systems as well as for isotopically superheavy pyrite of Neoproterozoic age. Our findings may fill the knowledge gap resulting from earlier sulfur cycling models that have predominantly focused on syn-depositional processes and organic matter sulfurization (Fike et al., 2015; Pasquier et al., 2017; Raven et al., 2019; Shawar et al., 2018), as well as burial diagenetic effects on sulfur isotopes (e.g., carbonate-associated sulfate [CAS] and pyrite; Drake et al., 2018; Fichtner et al., 2017), and have somewhat overlooked the isotopic impact of deep diagenesis (Figure 1).

2. Geological Setting

The Tarim Basin is an intracratonic basin surrounded by the Tianshan Mountains to the north, the Kunlun Mountains to the southwest, and the Algyn Mountains to the southeast (Figure 2a). During the Cambrian and Ordovician, the Tarim region evolved from an open platform (early Cambrian) to a restricted platform (middle to late Cambrian), then to an open platform (Ordovician), leading to the deposition of up to 2,000 m of sediments that are dominated by carbonates (Figure 2b). Evaporites (mainly anhydrite) are abundant in the lower to middle Cambrian strata throughout the entire basin (Figure 2b). Several orogenic events in the Tarim Basin led to basin-wide unconformities and karstification, denudation, as well as fracturing, tilting, localized volcanic activity, hydrocarbon charging, and hydrothermal events (Jiang et al., 2015a).

The burial and geothermal histories of different tectonic units in the Tarim Basin vary significantly (Jiang et al., 2016). In the subsurface, for example, the Tazhong area, the Cambrian-Ordovician strata were rapidly buried to depths greater than 5,000–8,000 m (with a maximum burial temperature of >200°C) before they were inverted and uplifted to depths ranging from 2,000 to 3,500 m (with a burial temperature of ~120°C) and followed by renewed subsidence to the current depth (~6,000–7,000 m and a burial temperature of ~180°C; Figure 2c; Jiang et al., 2016). Previous studies have documented that various types of diagenesis (e.g., meteoric and karstification, dolomitization, sulfate reduction, fracturing, brecciation, hydrothermal fluids related diagenesis, etc.) occurred in the Cambrian-Ordovician carbonate systems in the Tarim Basin (Figure 3; Cai et al., 2015a; Jia et al., 2015; Jiang et al., 2015a, 2018a).

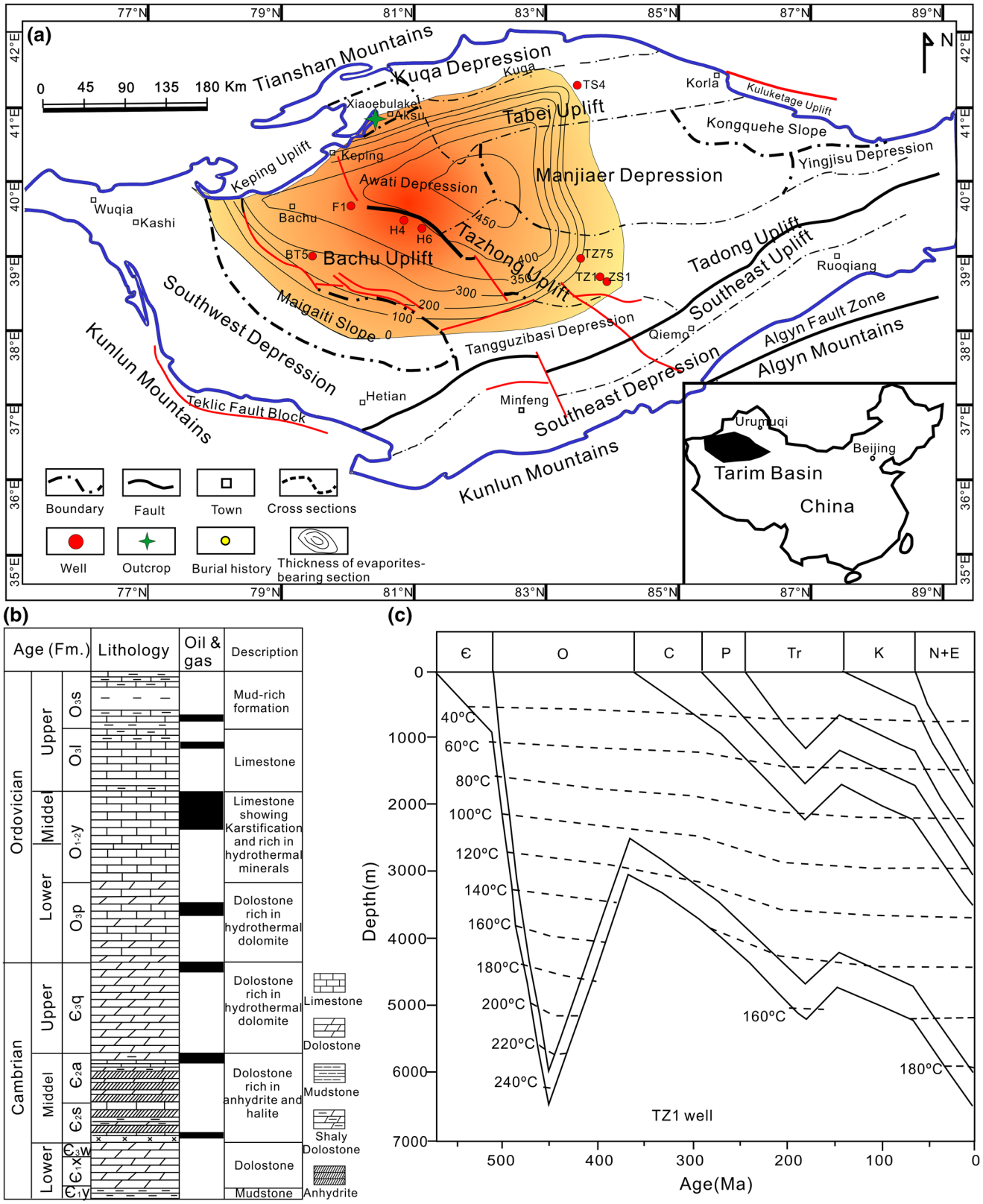

Figure 2. (a) Map of the Tarim Basin showing tectonic units, locations of sampled wells, and outcrops. The thickness of evaporites in the lower to middle Cambrian strata displaying a decreasing trend from the center to the edge of the basin. (b) A lithology column of Cambrian to Ordovician strata in the Tarim Basin. (c) A typical burial history diagram of the Cambrian to Ordovician units, well TZ1 from Tazhong area. (a) and (c) Modified from Jiang et al. (2016). (b) Modified from Jiang et al. (2015a).

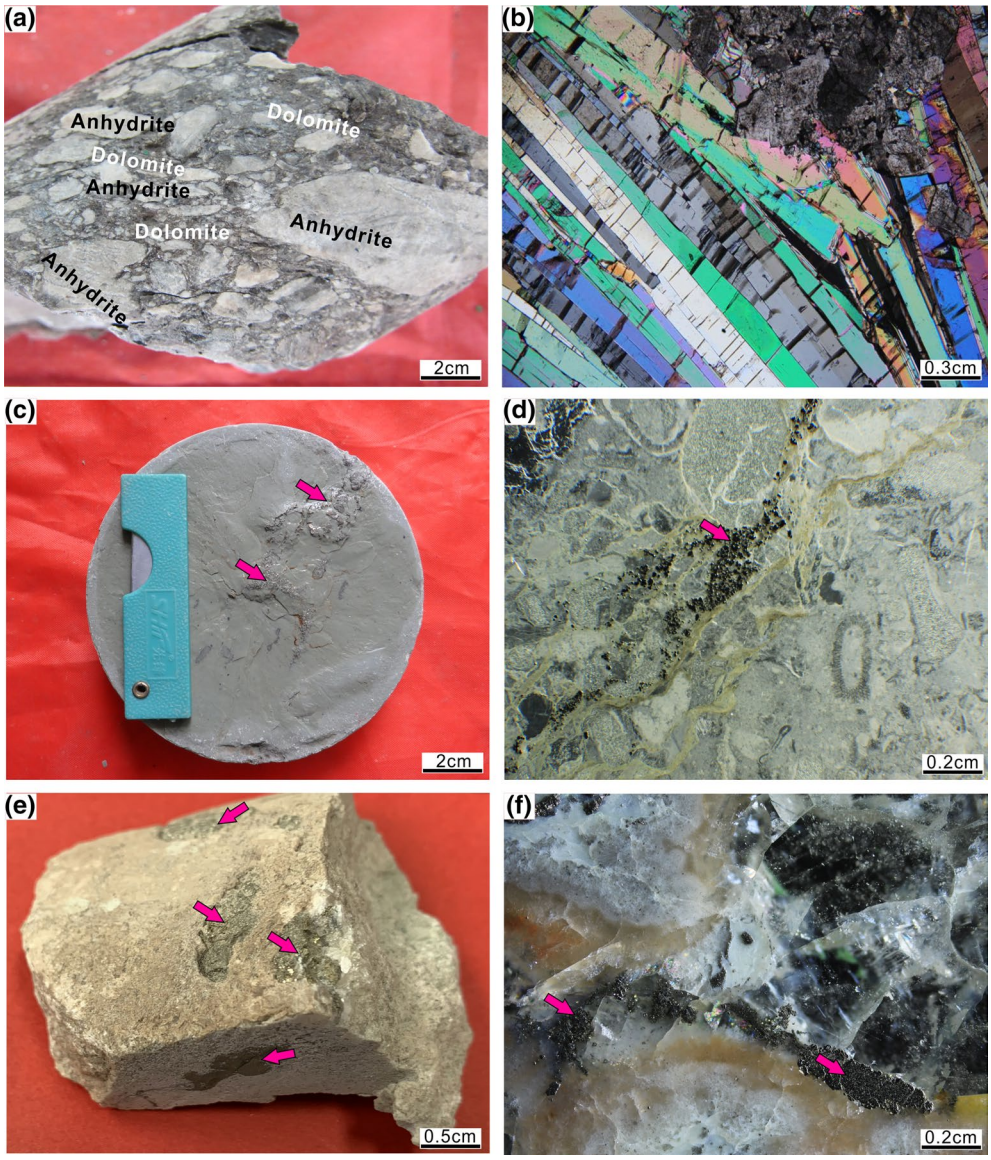

Figure 3. Photomicrographs showing various types of diagenetic pyrite (red arrow). (a) and (b) Display sedimentary versus diagenetic anhydrite. Diagenetic pyrite commonly occurs along with (c) fractures, (d) stylolites, and (e) pores and vugs. (f) These pyrites are commonly precipitated in association with diagenetic carbonate minerals.

3. Materials and Methods

3.1. Petrography

The main targets of this paper are the various types of sulfur-bearing species. In terms of petrography, we focus on diagenetic pyrite that is intergrown with diagenetic calcite and dolomite, which indicates that there is a temporal connection between the developments of pyrite and carbonate cement. Thin-section samples were made and stained with Alizarin Red S and potassium ferricyanide. They were studied using a Zeiss Axioskop 40A Pol light microscope to observe the occurrence of pyrite and to differentiate calcite, ferroan calcite, dolomite, and ferroan dolomite (Dickson, 1966).

3.2. Sulfur Isotopes

In this study, 10 sedimentary anhydrite samples were collected from the middle Cambrian strata in three exploration wells (well ZS5, BT5, and F1), 10 diagenetic anhydrite vein samples were collected from the

upper Cambrian unit from well TZ75, 29 diagenetic pyrite samples were collected from 14 well cores for sulfur isotope analyzes (Table S1). These pyrite samples occurred either as replacive or pore-filling pyrite.

Pyrite was liberated as H_2S with chromic chloride solution (Canfield et al., 1986). 0.1 M $AgNO_3$ was subsequently added to precipitate Ag_2S for stable S-isotope composition ($^{34}S/^{32}S$) analysis. The sulfur isotope ratios ($^{34}S/^{32}S$) of Ag_2S and $BaSO_4$ and anhydrite samples were determined using an Elementar Pyrocube elemental analyzer coupled to an Isoprime gas-sourced mass spectrometer operating in continuous flow mode. The $\delta^{34}S$ values were computed using the integrated m/z 64 and m/z 66 signals from each sample relative to the same mass intensities measured in a pulse of an independently introduced comparison SO_2. Calibration relative to the international Vienna-Canyon Diablo Troilite (VCDT) scale was accomplished using IAEA-S3 (sulfur isotopes in sphalerite) and an in-house seawater sulfate standard (SWS-3) that is isotopically indistinguishable from NBS-128 (sulfur isotopes in sphalerite). Analytical reproducibility, based on replicate measurement of calibration materials, is to be better 0.3%.

3.3. Fluid Inclusions Microthermometry

Homogenization temperatures (Th) were measured from fluid inclusion assemblages (FIAs) containing two-phase aqueous inclusions in five doubly polished (50–60 μm thick) wafers. The use of FIAs to determine temperatures of mineral growth, as opposed to lone inclusions, commonly shows each diagenetic mineral phase falls within a range of less than 10°C–15°C. This therefore gives confidence that the Th data are credible and minimizes the effects of artifacts, such as thermal re-equilibration (Goldstein, 2012; Goldstein & Reynolds, 1994). Fluid inclusion microthermometry was conducted using a Linkam THMSG 600 fluid inclusion stage mounted on a Zeiss Axioskop 40A Pol light microscope.

4. Results

4.1. Petrography

Two types of anhydrite were observed in the Cambrian-Ordovician carbonate systems. In detail, sedimentary anhydrite that occurs as nodules and thin (up to a few centimeters) layers (Figure 3a) is mainly presented in the lower to middle Cambrian strata. Whereas some diagenetic anhydrite with coarse crystals (Figure 3b) is typically associated with fractures in the upper Cambrian strata. Pyrite occurs as a pore- and, vug-, fracture-, and stylolite-filling mineral, which is predominantly intergrown with diagenetic carbonate minerals (Figures 3c–3f). These diagenetically formed types of pyrite display euhedral to subhedral crystals and have sizes from several micrometers and up to several millimeters (Figures 3c–3f).

4.2. Sulfur Isotopes

The $\delta^{34}S$ values of various types of sulfur-bearing species in the Cambrian-Ordovician carbonate hydrocarbon systems in the Tarim Basin varying by ~65‰, from −24.3% (in pyrite) to +40.4% VCDT (in barite) (Figure 4a; Table S1). Specifically, the sedimentary sulfate, present in the lower to middle Cambrian units, yields a narrow range of positive sulfur isotopic values between +28.9% and +34.1%, with an average at +32.0 ± 1.7% ($n = 10$). In contrast, replacive pyrite in the Ordovician units have a $\delta^{34}S$ range from −24.3% to −0.4%, with an average of −14.3 ± 7.9% ($n = 11$). Pore- and fracture-filling pyrite in the Ordovician units display a $\delta^{34}S$ range from +5.0% to +40.4%, with an average at +19.8 ± 9.8% ($n = 17$). Cambrian pyrite has relatively negative $\delta^{34}S$ values with a mean of approximately −20%, which is markedly lower than the Ordovician diagenetic pyrite (Figure 4). Other sulfur-bearing species including H_2S, oil, and kerogen S (Cai et al., 2015a, 2016), and diagenetic anhydrite (Jia et al., 2015) and barite (Cai et al., 2016), as well as aqueous sulfate in the formation waters (Li et al., 2017), from both the Cambrian and Ordovician carbonates, have also been compared (Figure 4).

4.3. Fluid Inclusions Microthermometry

Fifteen samples from several well cores (TZ 1, TZ 75, and ZS 5) and one outcrop (Xiaoerbulake) were selected for the fluid inclusion study. Among the studied sections, samples from well TZ1 were cored

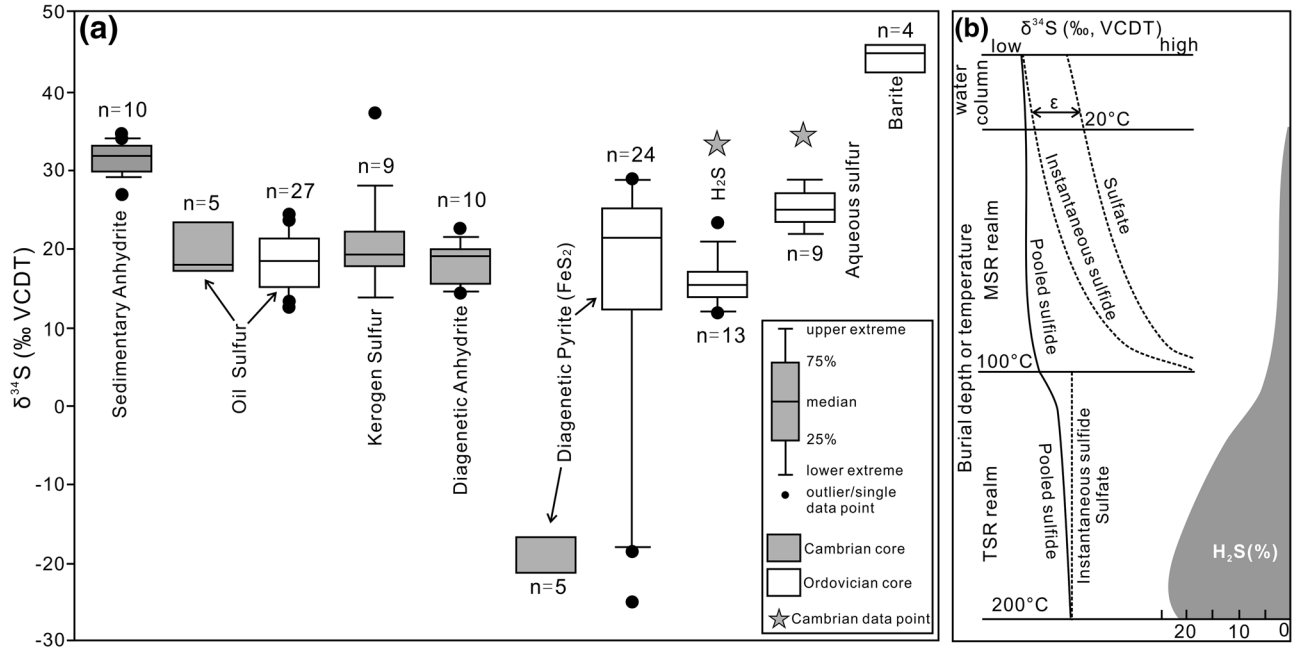

Figure 4. (a) Box-plot image showing $\delta^{34}S$ values of various types of diagenetic sulfur-bearing species and sedimentary sulfate in the Cambrian-Ordovician carbonate system from the Tarim Basin, NW China. (b) A sulfur cycling diagenesis model was built based on the data presented in (a). Note that an accumulated sulfur isotopic fractionation factor (ε) for MSR during diagenesis at temperatures <100°C, and little or no sulfur isotopic fractionation during the thermochemical sulfate reduction (TSR) diagenesis stage, was assumed. Increased $\delta^{34}S$ value of the H_2S pool in host carbonates was achieved due to Rayleigh fractionation in a relatively closed system. $\delta^{34}S$ values of H_2S, oil and kerogen sulfur, and barite were derived from Cai et al. (2009a), (2009b), (2015a), (2015b), and (2016), $\delta^{34}S$ values of diagenetic anhydrite were derived from Jia et al. (2015), and $\delta^{34}S$ values of aqueous sulfate were derived from Li et al. (2017).

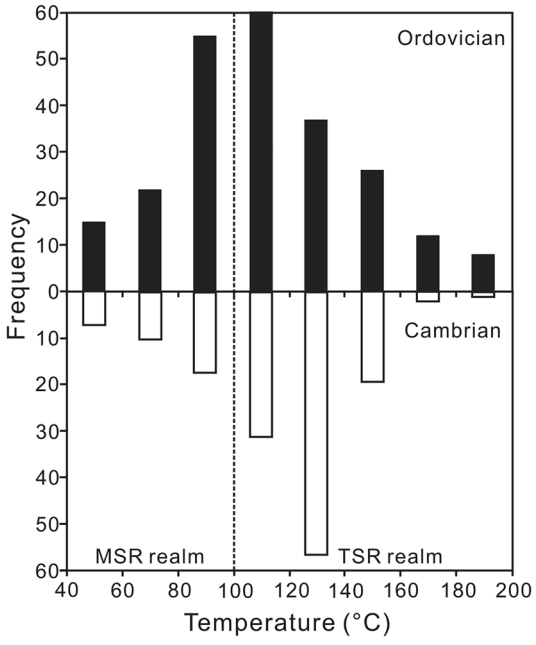

Figure 5. Histograms showing homogenization temperatures measured from fluid inclusions of diagenetic carbonates precipitated at microbial sulfate reduction (MSR) and thermochemical sulfate reduction (TSR) from the Cambrian-Ordovician units in Tarim Basin. In some locations, the intergrowth of diagenetic carbonates with diagenetic pyrite is observed.

from the Ordovician strata, whereas samples from well ZS 5 were cored from Cambrian strata, and cored samples from well TZ 75 and outcrop Xiaoerbulake cover both Ordovician and Cambrian strata. Abundant two-phase aqueous inclusions were present in diagenetic carbonate minerals, for example, the vug- and fracture-filling calcite and dolomite that is closely intergrown with diagenetic pyrite. Measured Th values or aqueous two-phase inclusions in FIAs in dolomite and calcite cement from the Cambrian-Ordovician carbonate system yield similar overall temperatures ranging from 40°C to 200°C. However, they demonstrate different temperature modes: the Ordovician mode is between 90°C and 110°C whereas the Cambrian mode falls around 130°C (Figure 5).

5. Discussion

Various types of S-bearing species that cover a wide $\delta^{34}S$ values range from ~ −25% to ~+47% have here been presented from the Cambrian-Ordovician carbonate system in the Tarim Basin (Figure 4). These S-bearing species were formed across the whole burial diagenesis realm according to burial temperatures obtained from fluid inclusion in diagenetic minerals (Figure 5). Multiple tectonic movements have induced basin-scale fluids to flow, including field-specific oil, and gas charging and migration. To add more complexity, the S-bearing species here may have been the mixing products of multiphase MSR and TSR.

5.1. Sulfur Cycling by Burial Diagenesis

Some replacive pyrite in the studied Cambrian-Ordovician carbonate systems is characterized by marked negative $\delta^{34}S$ values as low as −34.3%, suggesting MSR origins that are typically characterized by marked negative $\delta^{34}S$ value of < −40% (Canfield & Thamdrup, 1994; Sim et al., 2011). Sedimentary sulfate in the Cambrian-Ordovician carbonate stratigraphy is only present in the lower to middle Cambrian strata, which yields an average $\delta^{34}S$ value of ∼+32% (Figure 4; Table S1). The lowest precipitation temperatures (e.g., 55.7°C–73.2°C; Figure 5) measured from pyrite intergrowth with calcite suggests that isotopically light pyrite was formed through MSR (Machel, 2001) in a mesogenetic environment. We attribute this to the effect of in situ MSR in Ordovician strata, where sulfate was derived from the underlying Cambrian strata (Cai et al., 2015a). The enrichment of $\delta^{34}S$ values (from 42.1% to 46.6%) in barite cement (Figure 4a) was probably due to a Rayleigh distillation effect in an isotopically closed system (Figure 4b; Jørgensen, 1990). In contrast, the majority of diagenetic (pore-filling) pyrite and H_2S in the gas phases in the Ordovician strata display a narrow and positive $\delta^{34}S$ value range predominantly lying between ∼+15% and ∼+25% and are likely indicative of a TSR signal (Cai et al., 2016). These $\delta^{34}S$ values are somewhat (∼5%–15%) lighter than the Cambrian sulfate source (+31.6 ± 2.0%; Figure 4a) and broadly overlaps with the Ordovician seawater sulfur isotopic range (∼+20% to +30%; Kampschulte & Strauss, 2004). The latter source can be precluded due to the absence of sedimentary sulfate in the Ordovician strata. Further, any connate Ordovician seawater would have been diluted or replaced by meteoric water due to multiple denudation and karstification events that occurred in the Ordovician.

The relatively high temperatures (mainly between 80°C and 140°C) as obtained from some fluid inclusions in diagenetic minerals (e.g., calcite, dolomite, quartz, and fluorite; Figure 5), the dissolution of anhydrite, and precipitation of calcite (Jia et al., 2015), the presence of a relatively high volume of H_2S (Cai et al., 2015a), collectively support the occurrence of TSR. This might have contributed to the total amount of sulfide and consequently modified its $\delta^{34}S$ value (Krouse et al., 1988). However, high H_2S content (up to ∼ 8%–12%; Cai et al., 2015a) together with the broadly overlapping $\delta^{34}S$ values with oil-bearing sulfur (Figure 4a) provide credence for the idea that TSR has dominated the $\delta^{34}S$ signal over MSR in these diagenetic S-bearing species (Orr, 1974). Published burial history and fluid inclusion data have suggested that the Ordovician strata in the Tarim Basin reached the highest burial temperature of ∼200°C (Jia et al., 2015; Jiang et al., 2016). Published laboratory experimental data suggest that the $\Delta^{34}S_{sulfate\text{-}sulfide}$ value at equilibrium is ∼40% (Friedman & Neil, 1977) or ∼30% (Ohmoto, 1986; Ohmoto & Goldhaber, 1997; Ohmoto & Lasaga, 1982; Seal, 2006) at a temperature of ∼200°C, although lower and disequilibrium $\Delta^{34}S_{sulfate\text{-}sulfide}$ values (from −5.0% to 20.8%) have been reported in TSR experiments using amino acids (Watanabe et al., 2009). H_2S in the Cambrian strata is characterized by higher $\delta^{34}S$ values that are close to the Cambrian sulfate source (Figure 4a), suggesting that H_2S is derived from TSR in the studied system has imparted little isotope fractionation. We attribute the negligible ^{34}S isotope fractionation ($\Delta^{34}S_{sulfate\text{-}sulfide}$ = ∼0%) here, as well as at many deep burial anhydrite-rich carbonate and evaporite sections (Worden and Smalley, 1996) to be a common phenomenon through TSR diagenesis in sulfate-rich carbonate systems. The slightly depleted $\delta^{34}S$ values in sulfides from the Ordovician strata compared to the Cambrian sulfate source therefore implies mixing of H_2S generated by MSR and TSR during progressive burial.

5.2. Oxidation of Reduced Sulfur

The $\delta^{34}S$ values of SO_4^{2-} (water) in the Ordovician formation water is located in an intermediate range between Cambrian sedimentary sulfate and diagenetic sulfides (both H_2S and pyrite; Figure 4a), suggesting a likely mixing effect of ^{32}S-rich reduced S-compounds with ^{34}S-rich sulfate from the Cambrian strata. Geochemical characteristics (e.g., H, O, Sr, S isotopes, and water chemistry) of these formation waters suggest that aqueous SO_4^{2-} was predominantly derived from the dissolution of anhydrite in the underlying Cambrian strata (Li & Cai, 2017). However, $\delta^{34}S$ values of aqueous SO_4^{2-} are lower (up to ∼10%) than the anhydrite from Cambrian strata (Figure 4a). Sulfate should become increasingly enriched in ^{34}S as MSR continues in a closed diagenetic system with limited sulfate supplement. When entering the deep burial TSR diagenesis realm, $\delta^{34}S$ value of aqueous SO_4^{2-} may be unchanged because there is little net isotope fractionation. Therefore, the ^{34}S-depleted SO_4^{2-} (water) in the Ordovician strata are unlikely to be a direct product of residual aqueous SO_4^{2-} as a consequence of MSR or TSR. A ^{32}S-rich sulfate source may be introduced to the system by

(1) oxidation of existing H_2S, or (2) younger seawater with lower $\delta^{34}S$ values. The latter seems to be unlikely since the Ordovician strata may have been buried to depths up to several kilometers at the MSR diagenesis realm. Hence, the oxidation of H_2S formed by MSR was the most plausible scenario. Possible oxidation mechanisms for these reduced S-species during burial include: (1) cross-formation flow of fluids and (2) meteoric water influx caused by the regional tectonic events (Jiang et al., 2015a). Diagenetic anhydrite, which occurs as fracture fillings in the upper Cambrian strata (Figure 3), yields relatively negative $\delta^{34}S$ values (~5% lower than the current formation water), supporting the interpretation that oxidation of reduced S-species and mixing with the Cambrian sulfate is a plausible explanation. It has been suggested that diagenetic anhydrite precipitated at burial temperatures between 80°C and 120°C, corresponding to burial depths of ~1,500–2,700 m (Figure 1; Jia et al., 2015). Therefore, sulfur cycling by oxidation of sulfide during tectonic movements might have widely occurred and played an important role in regulating $\delta^{34}S$ value in aqueous SO_4^{2-}.

5.3. A Model for Sulfur Cycling Diagenesis

To quantify the isotopic effect of MSR and TSR on the $\delta^{34}S$ value of sedimentary sulfide, we have here developed a conceptional model for sulfur cycling during different stages of diagenesis (Figure 4b). We use the formulation described below to estimate the effect of MSR and TSR in the diagenesis zones (Equations 1–3). We assumed an initial $\delta^{34}S$ value of ~ +32% for the isotopic composition of aqueous sulfate (SO_4^{2-}) ($\delta^{34}S_{SO_4(\text{seawater})}$), according to the average $\delta^{34}S$ value of Cambrian sedimentary sulfate. As MSR proceeded, enrichment of ^{34}S in the residual sulfate pool can be expected due to the Rayleigh distillation effect in a closed system (Habicht et al., 1998; Jørgensen, 1990; Torfstein et al., 2005). An accumulated fractionation factor ($\varepsilon_{\text{pyrite-MSR}}$) can be calculated by considering $\delta^{34}S_{SO_4(\text{seawater})}$ minus the lightest $\delta^{34}S$ value for MSR diagenetic pyrite following Equation 1. Assuming that the maximum $\delta^{34}S$ values for aqueous SO_4^{2-} was the consequence of Rayleigh fractionation through MSR, and there is a relatively equal contribution to total pool of H_2S and pyrite from surface and deep sediment, the $\delta^{34}S$ value for pooled H_2S by MSR can be estimated following Equation 2. When entering the TSR diagenesis realm, the generated H_2S is characterized by enrichment in ^{34}S, with $\delta^{34}S$ values approaching the Cambrian sulfate ($\delta^{34}S$ = ~ +32%). The fraction of accumulated H_2S in the system from MSR (φ) and TSR $(1-\varphi)$ diagenesis can be further calculated according to Equation 3 providing that the $\delta^{34}S$ value of pooled H_2S_{MSR} is known.

$$\varepsilon_{\text{pyrite-MSR}} = \delta^{34}S_{SO_4(\text{seawater})} - \delta^{34}S_{\text{pyrite(min)}} \quad (1)$$

$$\delta^{34}S_{H_2S-\text{MSR(pooled)}} = \delta^{34}S_{\text{pyrite(min)}} + 0.5 \times \left[\delta^{34}S_{SO_4(\text{max})} - \delta^{34}S_{SO_4(\text{seawater})}\right] \quad (2)$$

$$\delta^{34}S_{H_2S} = \varphi \times \delta^{34}S_{H_2S-\text{MSR(pooled)}} + (1-\varphi) \times \delta^{34}S_{H_2S-TSR} \quad (3)$$

We have applied this new sulfur diagenesis model to quantitatively interpret the large variation of $\delta^{34}S$ values present in the Cambrian-Ordovician carbonate-dominated stratigraphy of the Tarim Basin (Figure 6a). An accumulated fractionation factor ($\varepsilon_{\text{pyrite-MSR}}$) of 50.5% can be calculated based on the lightest $\delta^{34}S$ value (~−18.5%) for MSR diagenetic pyrite in the studied interval (Equation 1; Table S1). A maximum $\delta^{34}S$ value of ~ +45% for aqueous SO_4^{2-} suggests that $\delta^{34}S$ enriched by 13% during MSR. A $\delta^{34}S$ value of −5.5% for accumulated H_2S during MSR diagenesis can be calculated according to Equation 2 (Figure 6a). The occurrence of multiple stages of the tectonic events may have led to multiphase MSR in the Cambrian-Ordovician carbonate system. The widespread distribution of diagenetic pyrite and H_2S may imply that if occurred the oxidation of sulfide, it should be a short-term event that has not significantly impacted the volume of reduced S-species. However, this localized, short-term, oxidation of H_2S may have depleted the $\delta^{34}S$ value in SO_4^{2-}. The presence of abundant H_2S in the gas phase also indicates the limited supply of metal ion (e.g., Fe^{2+}) to the system. When reaching the TSR diagenesis realm, the mixing of ^{34}S-rich H_2S_{TSR} with preexisting ^{32}S-rich H_2S_{MSR} lead to an increasing of $\delta^{34}S$ value in its accumulated H_2S. Therefore, pyrite precipitated from the accumulated H_2S during progressive burial would display a wide range and distinct $\delta^{34}S$ isotope values (Figure 7).

Assuming that the accumulated H_2S carried an average value of initial and final $\delta^{34}S$ values of MSR-sourced H_2S, the calculated isotopic composition of accumulated H_2S_{MSR} would become −12% (Equation 2). A simple

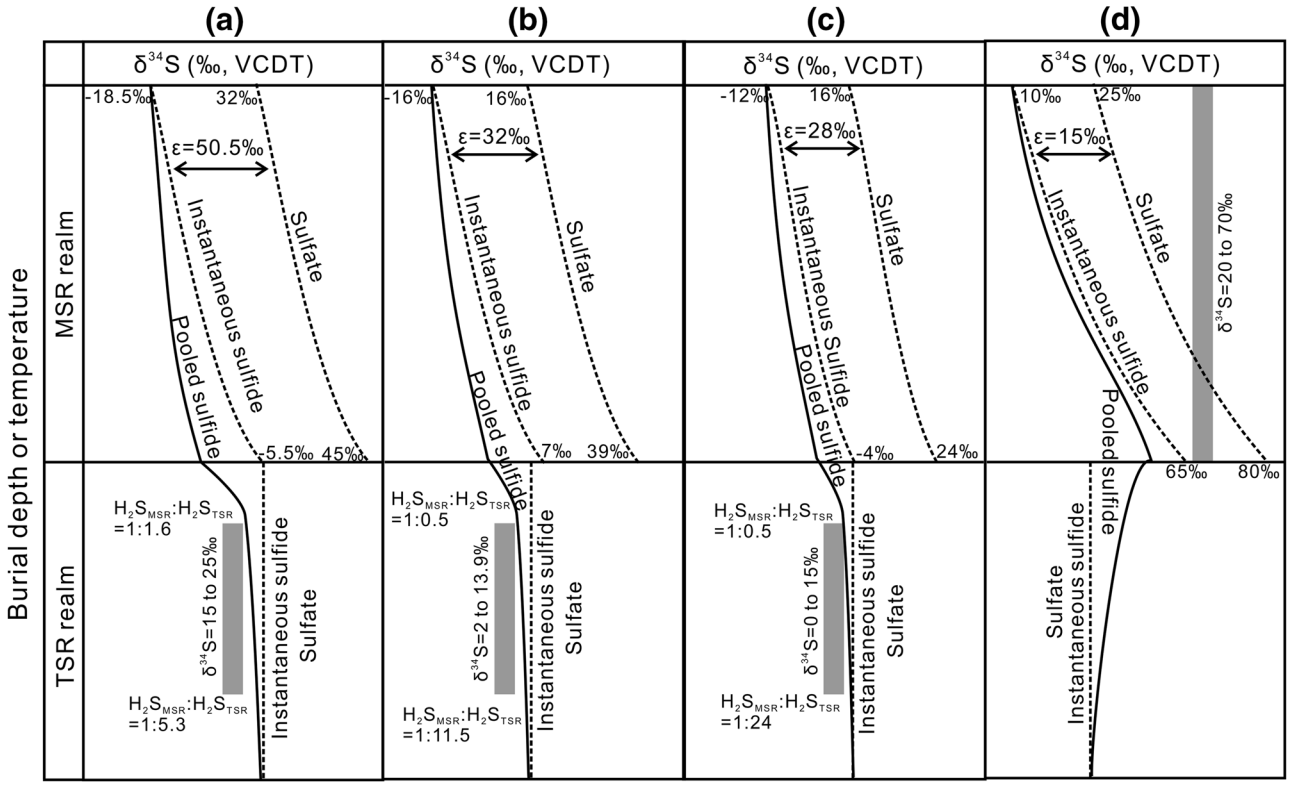

Figure 6. Applying the new sulfur cycling diagenesis model to interpret the $\delta^{34}S$ values for various types of sulfur-bearing species, in four global sedimentary basins, where sulfur cycling during diagenesis occurred. (a) The Cambrian-Ordovician carbonate system from the Tarim Basin, NW China, sulfate and sulfide data are derived from this study. (b) The Early Triassic Feixianguan Formation from the Sichuan Basin, China, sulfate and sulfide data are derived from Zhu et al. (2005) and Cai et al. (2010). (c) The Jurassic Smackover Formation from the Gulf of Mexico, US, sulfate and sulfide data are derived from Heydari and Moore (1989) and Moldovanyi et al. (1990). (d) The Neoproterozoic Datangpo Formation, South China. The gray bar shows the diagenesis realm for $\delta^{34}S$ values of sulfides generated by sulfate reductions in each carbonate system, H_2S_{MSR}: H_2S_{TSR} stands for the mixed volume ratio of H_2S generated by microbial sulfate reduction (MSR) or thermochemical sulfate reduction (TSR), which was calculated based on the lowest or highest $\delta^{34}S$ value of H_2S.

mass balance calculation suggests that mixing of (16%–39%) H_2S_{MSR} with (61%–84%) H_2S_{TSR}, with a volume ratio of H_2S_{MSR}: H_2S_{TSR} between 1–1.6 and 1–5.3, would result in $\delta^{34}S$ values of accumulated H_2S sitting between 15% and 25% in the studied Cambrian-Ordovician system (Equation 3; Figure 6a). Therefore, this new sulfur diagenesis model can be used to quantify the individual contributions of H_2S sourced from MSR and TSR in deeply-buried carbonate systems. We accept that there are limitations to this sulfur diagenesis model. For example, fractionation factor (ε) is assumed to be constant while more than one phase MSR may have occurred, and $\Delta^{34}S_{sulfate\text{-}sulfide}$ during TSR diagenesis is assumed to be ~0% in sulfate-rich carbonate systems, whereas $\Delta^{34}S_{sulfate\text{-}sulfide}$ for TSR could be much higher in sulfate limited conditions (Ohmoto, 1986; Ohmoto & Goldhaber, 1997; Ohmoto & Lasaga, 1982; Seal, 2006). MSR burial diagenesis with diminishing sulfate has been recently proposed to interpret the origin of superheavy pyrite in fractured continental bedrock in Sweden (Drake et al., 2018). However, it differs from the sulfur diagenesis model developed in this study, which is characterized by a more complicated diagenetic process with episodic sulfate reduction and sulfur cycling event. To our best knowledge, this is, so far, the most holistic understanding of the modulation of mixed $\delta^{34}S$ signals for accumulated H_2S generated from both MSR and TSR during progressive burial in hydrocarbon-bearing, sulfate-rich marine carbonate systems.

5.4. Implications for Sulfur Cycling During Mesodiagenesis (>100°C)

5.4.1. Implications for Sulfur Cycling in Sulfate-Rich Carbonate Petroleum Systems

Intending to quantify the contributions of MSR and TSR, we have applied our new sulfur diagenesis model to two other deeply buried marine carbonate systems: the Triassic Feixianguan Formation in the Sichuan

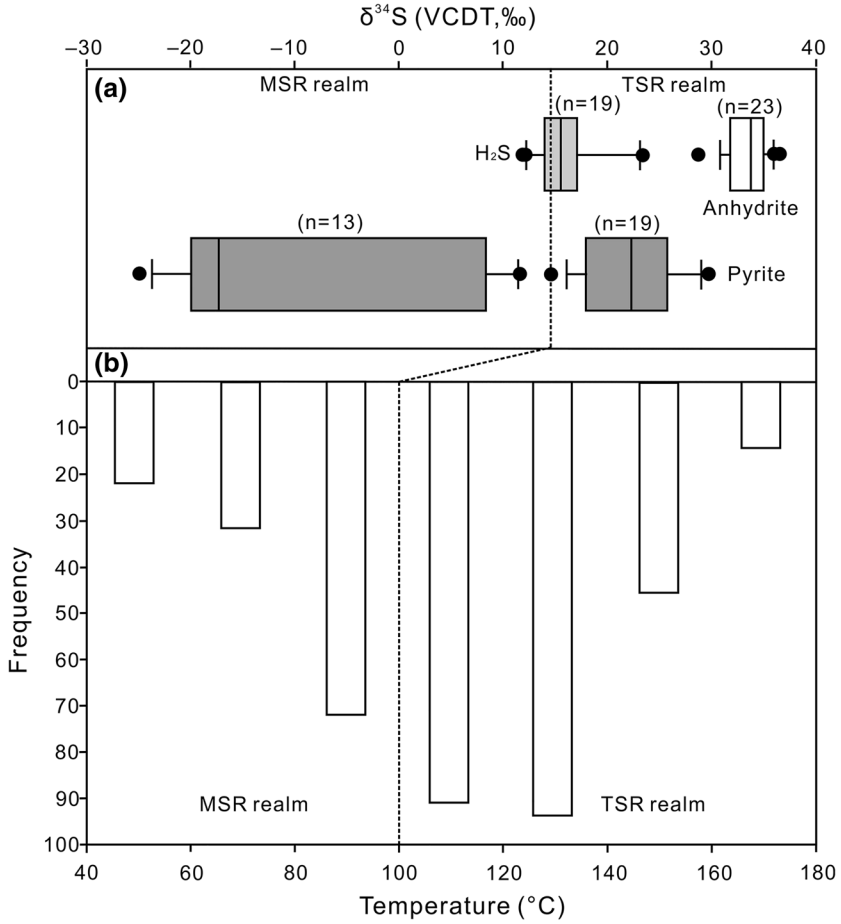

Figure 7. (a) Two end members of diagenetic pyrite which precipitated displaying distinct temperature and $\delta^{34}S$ isotopes range, whereas pooled H_2S showing $\delta^{34}S$ values in between suggest a mixing $\delta^{34}S$ signature of the above two end members. (b) Diagenetic temperatures for microbial sulfate reduction (MSR) and thermochemical sulfate reduction (TSR) diagenesis realms were aligned, temperature data were obtained from fluid inclusion in diagenetic carbonates.

Basin, China (Figure 6b; Table S2; Cai et al., 2010; Jiang et al., 2015b; Zhu et al., 2005) and the Jurassic Smackover Formation in Gulf of Mexico, US (Figure 6c; Table S2; Claypool & Mancini, 1989; Dworkin & Land, 1994; Gvirtzman et al., 2015; Heydari & Moore, 1989; Moldovanyi et al., 1990). TSR has been widely documented in these deeply-buried carbonate systems, where the effect of MSR on sulfur cycling may have been largely overlooked (Heydari & Moore, 1989; Krouse et al., 1988). The wide range of ^{34}S depleted phases (e.g., pyrite, elemental S, Oil-S, and H_2S) in these carbonate systems (Cai et al., 2010; Claypool & Mancini, 1989; Gvirtzman et al., 2015; Hao et al., 2008; Moldovanyi et al., 1990) support the occurrence of sulfur cycling during MSR diagenesis realm. Reduced sulfur-bearing phases (e.g., pyrite) with enriched ^{32}S values are most plausibly products of MSR. In contrast, reduced sulfur-bearing phases characterized with elevated $\delta^{34}S$ values, notably higher than the ones generated by MSR, are best interpreted by mixing of H_2S generated from TSR with the pre-existing H_2S generated by MSR (Figure 7). Following the same calculation as developed from the Cambrian-Ordovician system in the Tarim Basin, mixed H_2S_{MSR} and H_2S_{TSR} volume ratios varying from 1–0.5 to 1–11.5 and from 1–0.5 to 1–24 were calculated for the Triassic Feixianguan Formation and the Jurassic Smackover Formation, respectively (Figure 6). However, the varying fractionation factor (10%–57%) between the sulfate sources and sulfides among different basins (Figure 6) are likely due to variations in sulfate reduction rates, aqueous sulfate concentrations, and availability of aqueous sulfate and organic matter during MSR diagenesis (Canfield et al., 2010; Machel, 2001; Rudnicki et al., 2001).

The occurrence of MSR at eodiagenesis and TSR at mesodiagenesis environments could lead to a net volume loss by sulfate dissolution and calcite precipitation, and thus impact the carbonate hydrocarbon

reservoir qualities in the deep subsurface (Heydari & Moore, 1989; Jiang et al., 2015b, 2018a; Worden & Smalley, 1996). New porosity might be gained if calcite is transported out of the system. However, most of this new porosity is likely to be partially or wholly destroyed by later diagenesis (e.g., cementation or compaction). Hence, researchers have concluded that significant carbonate dissolution and enhanced carbonate reservoir quality by mesodiagenesis seems to be unlikely (Ehrenberg et al., 2012; Hao et al., 2008). However, some ideal cases have documented significant carbonate dissolution with an improved reservoir quality can be achieved by MSR diagenesis, for example, the Permian Units of the Permian Basin, USA (Mazzullo & Harris, 1991), as well as by TSR diagenesis, for example, the Triassic strata in the Sichuan Basin and Cambrian strata in the Tarim Basin, China (Cai et al., 2015a; Jiang et al., 2018b). Further, the accumulated H_2S and CO_2 by MSR and TSR are probably migrated to shallower carbonate strata via faults or fractures during tectonics. This may have resulted in H_2S tend to be oxidized, creating sulfuric acid, leading to significant dissolution of carbonates and the formation of caves for potential hydrocarbon reservoirs in the subsurface (Jiang et al., 2015a; Klimchouk, 2017).

5.4.2. Implications for Paleoclimate Reconstruction

Furthermore, we have re-evaluated the origin of relatively common, highly ^{34}S-enriched sedimentary sulfide in the Neoproterozoic, known as superheavy pyrite (Cui et al., 2018; Ries et al., 2009). While the origin of the superheavy pyrite is a matter of intense debate, a low seawater sulfate concentration coupled with intense aerobic re-oxidation of sedimentary sulfide has been invoked to explain the observed ^{34}S-rich sedimentary sulfide (Fike et al., 2015; Ries et al., 2009). However, petrographic characteristics such as the replacement of fine-grained host rock and the relatively coarse crystals of some pyrite grains (Cui et al., 2018; Wang et al., 2019) seems to support a burial diagenesis (mesodiagenesis) origin, rather than the syn-depositional origin. The TSR model for the generation of these superheavy pyrites (Cui et al., 2018) was further invoked based on the high-temperature data (average at 194°C) from diagenetic quartz present in the late fractures and veins in these sediments (Wang et al., 1985). However, these high-temperature fluid inclusion data are likely an indication of the maximum burial temperature, or a local hydrothermal event, rather than the reflection of the precipitation temperature for superheavy pyrite, which appears to have been generated at lower temperatures. Notably, superheavy pyrite formed by MSR in the burial diagenesis realm has been shown to have late diagenetic characteristics (Drake et al., 2018). Another important line of evidence, that led Cui et al. (2018) to deduce a TSR origin of the Datangpo superheavy pyrite, is the remarkably homogenous $\delta^{34}S$ values and the observation of decreasing $\delta^{34}S$ trend from core to edge of some individual pyrite grains, which is inconsistent with MSR but could be explained by TSR (Kiyosu & Krouse, 1990). Based on the local geology, anhydrite from the late-Ediacaran Dengying Formation with $\delta^{34}S$ value of ~ 40% (Friedman & Neil, 1977) was assumed to be the parent source of hydrothermal sulfate for the Datangpo TSR event (Cui et al., 2018). Models for pyrite precipitation in a closed system by Rayleigh distillation with an equilibrium value of 40% for $\Delta^{34}S_{sulfate\text{-}sulfide}$ could well explain the high $\delta^{34}S$ values of pyrite (Cui et al., 2018). A more recent parallel study of $\delta^{34}S$ values in pyrite and CAS has led Wang et al. (2019) to propose a new sulfur cycling model with ^{34}S-rich sulfide sourced from hydrothermal activity by reduction of older marine sulfates. However, they failed to provide any material evidence for hydrothermal activity as well as the reduction of older sulfate. The great variations of $\delta^{34}S$ values in CAS obtained from each studied sections (Wang et al., 2019) are probably an indication of diagenetic alteration. Thus, these CAS $\delta^{34}S$ values are more likely reflective of diagenetic pore-water signals rather than depositional seawater signatures.

The petrological features of these superheavy pyrites, for example, framboidal, interbedded texture, coarse crystals, and overgrowth, replacing matrix rocks, seem to imply that these superheavy pyrites were either syn-depositial or formed in the eodiagenesis MSR diagenesis realm. Hence, the sulfate source for MSR was most likely the Sturtian glaciation seawater. Abundant pyrite (Cui et al., 2018) and high concentrations of CAS (Wang et al., 2019) present in the Datangpo Formation are indicative of sulfate-rich system. By applying our new sulfur cycling diagenesis model and assuming a value of ~10% for the initial diagenetic sulfide and ~26% for $\delta^{34}S$ value of the Sturtian glaciation seawater sulfate (Gorjan et al., 2000), superheavy pyrite, with $\delta^{34}S$ values ranging predominantly from 50 to 70%, could only be precipitated in the MSR diagenesis realm (Figure 6d). Our proposed model is different to the near-surface diagenesis MSR model (Ries et al., 2009), the syn-depositional hydrothermal cycling of older marine sulfate model (Wang et al., 2019),

and the mesodiagenesis TSR model (Cui et al., 2018), and yet provides an alternative MSR diagenesis model that would have occurred at shallow burial environments with sulfate sources predominantly derived from the contemporaneous Sturtian glaciation seawater.

It is worth mentioning that carbonate authigenesis, promoted by MSR/AOM or methanogenesis during surface diagenesis, was a widespread and more significant global phenomenon in the Precambrian Era (e.g., Neoproterozoic) when the atmospheric O_2 concentration is widely viewed to be low (Laakso & Schrag, 2020; Lyons et al., 2014; Wood et al., 2019). This may have resulted in a large carbon isotope excursion in Neoproterozoic marine carbonates due to massive carbonate authigenesis (Laakso & Schrag, 2020; Schrag et al., 2013). We speculate that a large volume of accumulated H_2S, characterized by superheavy S-isotopes in the porous carbonate, has possibly occurred under eodiagenesis conditions. Convectional movement of H_2S can occur by regional conduits such as formation interfaces, faults, and nonconformities, as well as by diffusion; this led to superheavy pyrite precipitated as interlayer, pore-fracture-filling, and mineral overgrowth, for example, the ones observed in the Datangpo Formation (Cui et al., 2018). Late Neoproterozoic carbonates that are characterized by large global fluctuations present in $\delta^{34}S_{CAS}$, $\delta^{34}S_{pyr}$, and $\delta^{13}C_{carb}$ (Ries et al., 2009; Schrag et al., 2013) are crucial in the understanding of the origin and evolution of marine animal life (Wood et al., 2019). However, the global fluctuations of $\delta^{34}S$ and $\delta^{13}C$ during the Neoproterozoic could be the reflection of pore-water signals in sediments pile due to the extensive carbonate authigenesis (Jiang et al., 2019; Schrag et al., 2013), or large-scale precipitation of isotopically fractionated authigenic carbonates with oscillations in sulfate concentrations (Laakso & Schrag, 2020). The massive perturbations in $\delta^{13}C$ and $\delta^{34}S$ in marine carbonates do not necessary mirror changes in the global carbon and oxygen budgets, indeed, positive $\delta^{13}C$ values that are similar to the modern dissolved inorganic carbon has recently been reported to characterize the Neoproterozoic open sea (Hoffman & Lamothe, 2019). We argue that a profound examination of "diagenesis" is indispensable in gaining a better understanding of the primary signals of the deep-time marine carbonates, especially the Neoproterozoic ones that have co-occurred with the rise of marine metazoans.

6. Conclusions

The Cambrian-Ordovician carbonate units in the Tarim Basin, NW China, contains various types of sulfur-bearing components. To explore the isotopic effect of MSR and TSR on the isotopic composition of sedimentary sulfide, we herein developed a quantitative diagenetic model which can explain the sulfur isotope patterns in this sulfate-rich carbonate system. This model resulted from a detailed study of various types of sulfur-bearing species with distinct sulfur isotopes, coupled with a well-constrained diagenesis framework. To validate our new model, we applied it to two other deep burial sulfate-rich carbonate systems including the Triassic Feixianguan Formation, Sichuan Basin, China, and the Jurassic Smackover Formation, Gulf of Mexico Basin, USA, where widespread sulfate reduction and its associated sulfur cycling has occurred. Our new model quantifies the contribution of H_2S from both MSR and TSR and offers a new explanation for the observed wide range of sulfur isotopes from the Ordovician of the Tarim Basin, the Triassic of the Sichuan Basin, and the Jurassic of the Gulf of Mexico Basin. We suggest that this new sulfur cycling diagenesis model may be universal and applicable in most, or many, deeply-buried, ancient sulfate-rich carbonate systems. The model also provides an alternative, and more plausible, explanations for the origin of isotopically superheavy pyrite observed in Neoproterozoic sediments via shallow to intermediate burial MSR at eodiagenesis realm (<70°C).

Acknowledgments
This paper was financially supported by projects from the National Key Research and Development Project (2019YFB1504101), National Science Foundation of China (41972149; 41890843), Key Research Program of the Institute of Geology & Geophysics, CAS, Grant No. IGGCAS-201903, PetroChina Innovation Foundation, and Youth Innovation Promotion Association of the Chinese Academy of Sciences (2018088). The authors are graterful for constructive and critical comments from the reviewer Huan Cui and two anonymous reviewers, and detailed comments and instructions from editor Branwen Williams.

Data Availability Statement

Data archiving has been uploaded to http://www.dx.doi.org/10.12197/2020GA017. (URL: http://www.geophys.ac.cn/ArticleDataInfo.asp?MetaId=216, DOI: https://doi.org/10.12197/2020GA017.)

References

Bildstein, O., Worden, R. H., & Brosse, E. (2001). Assessment of anhydrite dissolution as the rate-limiting step during thermochemical sulphate reduction. *Chemical Geology*, *176*(1–4), 173–189.

Böttcher, M. E., Sievert, S. M., & Kuever, J. (1999). Fractionation of sulfur isotopes during dissimilatory reduction of sulphate by a thermophilic gram-negative bacterium at 60° C. *Archives of Microbiology*, *172*(2), 125–128.
Bradley, A. S., Leavitt, W. D., Schmidt, M., Knoll, A. H., Girguis, P. R., & Johnston, D. T. (2016). Patterns of sulfur isotope fractionation during microbial sulphate reduction. *Geobiology*, *14*(1), 91–101. https://doi.org/10.1111/gbi.12149
Bryant, R. N., Jones, C., Raven, M. R., Gomes, M. L., Berelson, W. M., Bradley, A. S., et al. (2019). Sulfur isotope analysis of microcrystalline iron sulfides using secondary ion mass spectrometry imaging: Extracting local paleo-environmental information from modern and ancient sediments. *Rapid Communications in Mass Spectrometry*, *33*(5), 491–502. https://doi.org/10.1002/rcm.8375
Cai, C., Amrani, A., Worden, R. H., Xiao, Q., Wang, T., Gvirtzman, Z., et al. (2016). Sulfur isotopic compositions of individual organosulfur compounds and their genetic links in the Lower Paleozoic petroleum pools of the Tarim Basin, NW China. *Geochimica et Cosmochimica Acta*, *182*, 88–108. https://doi.org/10.1016/j.gca.2016.02.036
Cai, C., Hu, G. Y., Li, H. X., Jiang, L., He, W. X., Zhang, B. S., et al. (2015a). Origins and fates of H_2S in the Cambrian and Ordovician in Tazhong area: Evidence from sulfur isotopes, fluid inclusions and production data. *Marine and Petroleum Geology*, *67*, 408–418. https://doi.org/10.1016/j.marpetgeo.2015.05.007
Cai, C., Li, K., Anlai, M., Zhang, C., Xu, Z., Worden, R. H., et al. (2009a). Distinguishing Cambrian from Upper Ordovician source rocks: Evidence from sulfur isotopes and biomarkers in the Tarim Basin. *Organic Geochemistry*, *40*(7), 755–768. https://doi.org/10.1016/j.orggeochem.2009.04.008
Cai, C., Li, K., Zhu, Y., Xiang, L., Jiang, L., Cai, X., et al. (2010). TSR origin of sulfur in Permian and Triassic reservoir bitumen, East Sichuan Basin, China. *Organic Geochemistry*, *41*(9), 871–878. https://doi.org/10.1016/j.orggeochem.2010.03.009
Cai, C., Zhang, C., Cai, L., Wu, G., Jiang, L., Xu, Z., et al. (2009b). Origins of Palaeozoic oils in the Tarim Basin: Evidence from sulfur isotopes and biomarkers. *Chemical Geology*, *268*(3), 197–210. https://doi.org/10.1016/j.chemgeo.2009.08.012
Cai, C., Zhang, C., Worden, R. H., Wang, T., Li, H., Jiang, L., et al. (2015b). Application of sulfur and carbon isotopes to oil–source rock correlation: A case study from the Tazhong area, Tarim Basin, China. *Organic Geochemistry*, *83–84*, 140–152. https://doi.org/10.1016/j.orggeochem.2015.03.012
Canfield, D. E., Farquhar, J., & Zerkle, A. L. (2010). High isotope fractionations during sulphate reduction in a low-sulphate euxinic ocean analog. *Geology*, *38*(5), 415–418. https://doi.org/10.1130/G30723.1
Canfield, D. E., Raiswell, R., Westrich, J. T., Reaves, C. M., & Berner, R. A. (1986). The use of chromium reduction in the analysis of reduced inorganic sulfur in sediments and shales. *Chemical Geology*, *54*(1–2), 149–155.
Canfield, D. E., & Teske, A. (1996). Late Proterozoic rise in atmospheric oxygen concentration inferred from phylogenetic and sulphur-isotope studies. *Nature*, *382*(6587), 127.
Canfield, D. E., & Thamdrup, B. (1994). The production of (34) S-depleted sulfide during bacterial disproportionation of elemental sulfur. *Science*, *266*(5193), 1973.
Claypool, G. E. (2004), Ventilation of marine sediments indicated by depth profiles of pore water sulphate and δ34S. In R. J. Hill, J. Leventhal, Z. Aizenshtat, M. J. Baedecker, G. Claypool, R. Eganhouse, M. Goldhaber, & K. Peters (Eds.), *The geochemical society special publications* (Vol. 9, pp. 59–65). Amsterdam, Netherlands: Elsevier. https://doi.org/10.1016/S1873-9881(04)80007-5
Claypool, G. E., Holser, W. T., Kaplan, I. R., Sakai, H., & Zak, I. (1980). The age curves of sulfur and oxygen isotopes in marine sulphate and their mutual interpretation. *Chemical Geology*, *28*, 199–260.
Claypool, G. E., & Mancini, E. A. (1989). Geochemical relationships of petroleum in Mesozoic reservoirs to carbonate source rocks of Jurassic Smackover Formation, southwestern Alabama. *AAPG Bulletin*, *73*(7), 904–924.
Cui, H., Kitajima, K., Spicuzza, M. J., Fournelle, J. H., Denny, A., Ishida, A., et al. (2018). Questioning the biogenicity of Neoproterozoic superheavy pyrite by SIMS. *American Mineralogist: Journal of Earth and Planetary Materials*, *103*(9), 1362–1400. https://doi.org/10.2138/am-2018-6489
Dickson, J. (1966). Carbonate identification and genesis as revealed by staining. *Journal of Sedimentary Research*, *36*(2), 491–505.
Drake, H., Whitehouse, M. J., Heim, C., Reiners, P. W., Tillberg, M., Hogmalm, K. J., et al. (2018). Unprecedented 34S-enrichment of pyrite formed following microbial sulphate reduction in fractured crystalline rocks. *Geobiology*, *16*(5), 556–574. https://doi.org/10.1111/gbi.12297
Dworkin, S., & Land, L. (1994). Petrographic and geochemical constraints on the formation and diagenesis of anhydrite cements, Smackover sandstones, Gulf of Mexico. *Journal of Sedimentary Research*, *64*(2a), 339–348.
Ehrenberg, S. N., Walderhaug, O., & Bjørlykke, K. (2012). Carbonate porosity creation by mesogenetic dissolution: Reality or illusion? *AAPG Bulletin*, *96*(2), 217–233. https://doi.org/10.1306/05031110187
Fichtner, V., Strauss, H., Immenhauser, A., Buhl, D., Neuser, R. D., & Niedermayr, A. (2017). Diagenesis of carbonate associated sulphate. *Chemical Geology*, *463*, 61–75. https://doi.org/10.1016/j.chemgeo.2017.05.008
Fike, D. A., Bradley, A. S., & Rose, C. V. (2015). Rethinking the ancient sulfur cycle. *Annual Review of Earth and Planetary Sciences*, *43*, 593–622. https://doi.org/10.1146/annurev-earth-060313-054802
Friedman, I. O., & Neil, J. R. (1977). M. Fleischer *Compilation of Stable Isotope Fractionation Factors of Geochemical Interest*, Data of Geochemistry Professional Paper 440kk, (1–12). Reston, Virginia: U.S. Geological Survey.
Goldstein, R. (2012). Fluid inclusion geothermometry in sedimentary systems: From paleoclimate to hydrothermal. In R. Goldstein & J. Reynolds (Eds.), *Thermal history analysis of sedimentary basins* (Vol. 103, pp. 45–63). https://doi.org/10.2110/sepmsp.103
Goldstein, R., & Reynolds, T. J. (1994). Systematics of fluid inclusions in diagenetic minerals. *SEPM Short Course Notes*, *31*, 199.
Gorjan, P., Veevers, J. J., & Walter, M. R. (2000). Neoproterozoic sulfur-isotope variation in Australia and global implications. *Precambrian Research*, *100*(1), 151–179. https://doi.org/10.1016/S0301-9268(99)00073-X
Gvirtzman, Z., Said-Ahmad, W., Ellis, G. S., Hill, R. J., Moldowan, J. M., Wei, Z., et al. (2015). Compound-specific sulfur isotope analysis of thiadiamondoids of oils from the Smackover Formation, USA. *Geochimica et Cosmochimica Acta*, *167*, 144–161. https://doi.org/10.1016/j.gca.2015.07.008
Habicht, K. S., Canfield, D. E., & Rethmeier, J. o. (1998). Sulfur isotope fractionation during bacterial reduction and disproportionation of thiosulfate and sulfite. *Geochimica et Cosmochimica Acta*, *62*(15), 2585–2595.
Hao, F., Guo, T., Zhu, Y., Cai, X., Zou, H., & Li, P. (2008). Evidence for multiple stages of oil cracking and thermochemical sulphate reduction in the Puguang gas field, Sichuan Basin, China. *AAPG Bulletin*, *92*(5), 611–637. https://doi.org/10.1306/01210807090
Heydari, E., & Moore, C. H. (1989). Burial diagenesis and thermochemical sulphate reduction, Smackover Formation, southeastern Mississippi salt basin. *Geology*, *17*(12), 1080–1084.
Hoffman, P. F., & Lamothe, K. G. (2019). Seawater-buffered diagenesis, destruction of carbon isotope excursions, and the composition of DIC in Neoproterozoic oceans. *Proceedings of the National Academy of Sciences of the United States of America*, *116*(38), 18874–18879. https://doi.org/10.1073/pnas.1909570116

Holser, W., & Kaplan, I. (1966). Isotope geochemistry of sedimentary sulfates. *Chemical Geology*, *1*, 93–135.
Jia, L., Cai, C., Yang, H., Li, H., Wang, T., Zhang, B., et al. (2015). Thermochemical and bacterial sulphate reduction in the Cambrian and Lower Ordovician carbonates in the Tazhong Area, Tarim Basin, NW China: Evidence from fluid inclusions, C, S, and Sr isotopic data. *Geofluids*, *15*(3), 421–437. https://doi.org/10.1111/gfl.12105
Jiang, L., Cai, C. F., Worden, R. H., Crowley, S. F., Jia, L. Q., Zhang, K., et al. (2016). Multiphase dolomitization of deeply buried Cambrian petroleum reservoirs, Tarim Basin, north-west China. *Sedimentology*, *63*(7), 2130–2157. https://doi.org/10.1111/sed.12300
Jiang, L., Pan, W. Q., Cai, C. F., Jia, L. Q., Pan, L. Y., Wang, T. K., et al. (2015a). Fluid mixing induced by hydrothermal activity in the ordovician carbonates in Tarim Basin, China. *Geofluids*, *15*, 483–498. https://doi.org/10.1111/gfl.12125
Jiang, L., Planavsky, N., Zhao, M., Liu, W., & Wang, X. (2019). Authigenic origin for a massive negative carbon isotope excursion. *Geology*, *47*(2), 115–118. https://doi.org/10.1130/g45709.1
Jiang, L., Worden, R. H., & Cai, C. (2015b). Generation of isotopically and compositionally distinct water during thermochemical sulphate reduction (TSR) in carbonate reservoirs: Triassic Feixianguan Formation, Sichuan Basin, China. *Geochimica et Cosmochimica Acta*, *165*, 249–262. https://doi.org/10.1016/j.gca.2015.05.033
Jiang, L., Worden, R. H., Cai, C. F., Shen, A., & Crowley, S. F. (2018a). Diagenesis of an evaporite-related carbonate reservoir in deeply buried Cambrian strata, Tarim Basin, northwest China. *AAPG Bulletin*, *102*(1), 77–102. https://doi.org/10.1306/0328171608517048
Jiang, L., Worden, R. H., & Yang, C. (2018b). Thermochemical sulphate reduction can improve carbonate petroleum reservoir quality. *Geochimica et Cosmochimica Acta*, *223*, 127–140. https://doi.org/10.1016/j.gca.2017.11.032
Jorgensen, B. B. (1979). A theoretical model of the stable sulfur isotope distribution in marine sediments. *Geochimica et Cosmochimica Acta*, *43*(3), 363–374. https://doi.org/10.1016/0016-7037(79)90201-1
Jørgensen, B. B. (1990). A thiosulfate shunt in the sulfur cycle of marine sediments. *Science*, *249*(4965), 152–154.
Kampschulte, A., & Strauss, H. (2004). The sulfur isotopic evolution of Phanerozoic seawater based on the analysis of structurally substituted sulphate in carbonates. *Chemical Geology*, *204*(3), 255–286. https://doi.org/10.1016/j.chemgeo.2003.11.013
Kiyosu, Y. (1980). Chemical reduction and sulfur-isotope effects of sulphate by organic matter under hydrothermal conditions. *Chemical Geology*, *30*(1), 47–56. https://doi.org/10.1016/0009-2541(80)90115-1
Kiyosu, Y., & Krouse, H. R. (1990). The role of organic acid in the abiogenic reduction of sulphate and the sulfur isotope effect. *Geochemical Journal*, *24*(1), 21–27. https://doi.org/10.2343/geochemj.24.21
Klimchouk, A. (2017). Types and settings of hypogene karst. In A. Klimchouk, A. N. Palmer, J. De Waele, A. S. Auler, & P. Audra (Eds.), *Hypogene karst regions and caves of the world* (pp. 1–39). Cham, Switzerland: Springer International Publishing. https://doi.org/10.1007/978-3-319-53348-3_1
Krouse, H. R., Viau, C. A., Eliuk, L. S., Ueda, A., & Halas, S. (1988). Chemical and isotopic evidence of thermochemical sulphate reduction by light hydrocarbon gases in deep carbonate reservoirs. *Nature*, *333*, 415–419.
Laakso, T. A., & Schrag, D. P. (2020). The role of authigenic carbonate in Neoproterozoic carbon isotope excursions. *Earth and Planetary Science Letters*, *549*, 116534. https://doi.org/10.1016/j.epsl.2020.116534
Li, H., & Cai, C. (2017). Origin and evolution of formation water from the Ordovician carbonate reservoir in the Tazhong area, Tarim Basin, NW China. *Journal of Petroleum Science and Engineering*, *148*, 103–114. https://doi.org/10.1016/j.petrol.2016.10.016
Li, H., Cai, C., Jia, L., Xu, C., & Zhang, K. (2017). The effect of water chemistry on thermochemical sulphate reduction: A case study from the Ordovician in the Tazhong area, Northwest China. *Geofluids. 2017*, 1–11. https://doi.org/10.1155/2017/6351382
Lyons, T. W., Reinhard, C. T., & Planavsky, N. J. (2014). The rise of oxygen in Earth's early ocean and atmosphere. *Nature*, *506*(7488), 307. https://doi.org/10.1038/nature13068
Machel, H. G. (2001). Bacterial and thermochemical sulphate reduction in diagenetic settings—old and new insights. *Sedimentary Geology*, *140*(1), 143–175.
Masterson, A., Alperin, M. J., Berelson, W. M., & Johnston, D. T. (2018). Interpreting multiple sulfur isotope signals in modern anoxic sediments using a full diagenetic model (California-Mexico margin: Alfonso Basin). *American Journal of Science*, *318*(5), 459–490. https://doi.org/10.2475/05.2018.02
Mazzullo, S. J., & Harris, P. M. (1991). An overview of dissolution porosity development in the deep-burial environment, with examples from carbonate reservoirs in the Permian Basin. In M. P. Candelaria (Ed.), *Permian Basin Plays – Tomorrow's Technology Today* (Vol. 91-89, pp. 125–138). Midland, TX: West Texas Geological Society.
Moldovanyi, E. P., Walter, L. M., Brannon, J. C., & Podosek, F. A. (1990). New constraints on carbonate diagenesis from integrated Sr and S isotopic and rare earth element data, Jurassic Smackover Formation, US Gulf Coast, *Applied Geochemistry*, *5*(4), 449–470.
Ohmoto, H. (1986). Stable isotope geochemistry of ore deposits. In J. W. Valley, H. P. Taylor, & J. R. O'Neil (Eds.), *Stable isotopes in high temperature geological processes, reviews in mineralogy* (Vol. 16, pp. 491–559). Denver, CO: Mineralogical Society of America.
Ohmoto, H., & Goldhaber, M. B. (1997). Sulfur and carbon isotopes. In H. L. Barnes (Ed.), *Geochemistry of hydrothermal ore deposits* (3rd ed., pp. 517–611). New York, NY: John Wiley & Sons.
Ohmoto, H., & Lasaga, A. C. (1982). Kinetics of reactions between aqueous sulfates and sulfides in hydrothermal systems. *Geochimica et Cosmochimica Acta*, *46*(10), 1727–1745. https://doi.org/10.1016/0016-7037(82)90113-2
Orr, W. L. (1974). Changes in sulfur content and isotopic ratios of sulfur during petroleum maturation – study of Big Horn basin Paleozoic oils. *AAPG Bulletin*, *58*(11), 2295–2318.
Pasquier, V., Sansjofre, P., Rabineau, M., Revillon, S., Houghton, J., & Fike, D. A. (2017). Pyrite sulfur isotopes reveal glacial – interglacial environmental changes. *Proceedings of the National Academy of Sciences of the United States of America*, *114*(23), 5941–5945. https://doi.org/10.1073/pnas.1618245114
Raven, M. R., Fike, D. A., Bradley, A. S., Gomes, M. L., Owens, J. D., & Webb, S. A. (2019). Paired organic matter and pyrite δ34S records reveal mechanisms of carbon, sulfur, and iron cycle disruption during Ocean Anoxic Event 2. *Earth and Planetary Science Letters*, *512*, 27–38. https://doi.org/10.1016/j.epsl.2019.01.048
Ries, J. B., Fike, D. A., Pratt, L. M., Lyons, T. W., & Grotzinger, J. P. (2009). Superheavy pyrite (δ34Spyr> δ34SCAS) in the terminal Proterozoic Nama Group, southern Namibia: A consequence of low seawater sulphate at the dawn of animal life. *Geology*, *37*(8), 743–746. https://doi.org/10.1130/G25775A.1
Rudnicki, M. D., Elderfield, H., & Spiro, B. (2001). Fractionation of sulfur isotopes during bacterial sulphate reduction in deep ocean sediments at elevated temperatures. *Geochimica et Cosmochimica Acta*, *65*(5), 777–789.
Schrag, D. P., Higgins, J. A., Macdonald, F. A., & Johnston, D. T. (2013). Authigenic carbonate and the history of the global carbon cycle. *Science*, *339*(6119), 540–543. https://doi.org/10.1126/science.1229578
Seal, R. R. II (2006). Sulfur isotope geochemistry of sulfide minerals. *Reviews in Mineralogy and Geochemistry*, *61*(1), 633–677. https://doi.org/10.2138/rmg.2006.61.12

Shawar, L., Halevy, I., Said-Ahmad, W., Feinstein, S., Boyko, V., Kamyshny, A., et al. (2018). Dynamics of pyrite formation and organic matter sulphurization in organic-rich carbonate sediments. *Geochimica et Cosmochimica Acta*, *241*, 219–239. https://doi.org/10.1016/j.gca.2018.08.048

Sim, M. S., Bosak, T., & Ono, S. (2011). Large sulfur isotope fractionation does not require disproportionation. *Science*, *333*(6038), 74–77. https://doi.org/10.1126/science.1205103

Thode, H. G., & Monster, J. (1965). Sulfur-isotope geochemistry of petroleum, evaporites, and ancient seas. In A. Young & J. E. Galley (Eds.) *AAPG memoirs 4: Fluids in subsurface environments* (pp. 367–377). Tulsa, OK:).American Association of Petroleum Geologists.

Torfstein, A., Gavrieli, I., & Stein, M. (2005). The sources and evolution of sulfur in the hypersaline Lake Lisan (paleo-Dead Sea). *Earth and Planetary Science Letters*, *236*(1–2), 61–77. https://doi.org/10.1016/j.epsl.2005.04.026

Wang, P., Algeo, T. J., Zhou, Q., Yu, W., Du, Y., Qin, Y., et al. (2019). Large accumulations of 34S-enriched pyrite in a low-sulphate marine basin: The Sturtian Nanhua Basin, South China. *Precambrian Research*, *335*, 105504. https://doi.org/10.1016/j.precamres.2019.105504

Wang, Y., Wang, L., & Zhu, S. (1985). *The stratigraphy, sedimentary environment and manganese-forming process of the Datangpo Formation in Eastern Guizhouu*. Guiyang: People's Publishing House of Guizhou. (in Chinese.)

Watanabe, Y., Farquhar, J., & Ohmoto, H. (2009). Anomalous fractionations of sulfur isotopes during thermochemical sulphate reduction. *Science*, *324*(5925), 370–373. https://doi.org/10.1126/science.1169289

Wing, B. A., & Halevy, I. (2014). Intracellular metabolite levels shape sulfur isotope fractionation during microbial sulphate respiration. *Proceedings of the National Academy of Sciences of the United States of America*, *111*(51), 18116–18125. https://doi.org/10.1073/pnas.1407502111

Wood, R., Liu, A. G., Bowyer, F., Wilby, P. R., Dunn, F. S., Kenchington, C. G., et al. (2019). Integrated records of environmental change and evolution challenge the Cambrian Explosion. *Nature Ecology & Evolution*, *3*, 528–538. https://doi.org/10.1038/s41559-019-0821-6

Worden, R., Armitage, P. J., Butcher, A. R., Churchill, J. M., Csoma, A. E., Hollis, C., et al. (2018). Petroleum reservoir quality prediction: Overview and contrasting approaches from sandstone and carbonate communities. *Geological Society, London, Special Publications*, *435*(1), 1–31. https://doi.org/10.1144/SP435.21

Worden, R. H., & Smalley, P. C. (1996). H_2S-producing reactions in deep carbonate gas reservoirs: Khuff Formation, Abu Dhabi. *Chemical Geology*, *133*(1–4), 157–171.

Worden, R., Smalley, P. C., & Fallick, A. E. (1997). Sulfur cycle in buried evaporites. *Geology*, *25*(7), 643–646.

Wortmann, U. G., Bernasconi, S. M., & Böttcher, M. E. (2001). Hypersulfidic deep biosphere indicates extreme sulfur isotope fractionation during single-step microbial sulphate reduction. *Geology*, *29*(7), 647–650.

Zhu, G., Zhang, S., Liang, Y., Dai, J., & Li, J. (2005). Isotopic evidence of TSR origin for natural gas bearing high H 2 S contents within the Feixianguan Formation of the northeastern Sichuan Basin, southwestern China. *Science in China - Series D: Earth Sciences*, *48*(11), 1960. https://doi.org/10.1360/082004-147